Vacuum 202 (2022) 111130

Contents lists available at ScienceDirect

Vacuum

journal homepage: www.elsevier.com/locate/vacuum

Effects of As, P and Sb on the output voltage generation of ZnO nanowires based nanogenerator: Mitigation of screening effect by using surface modified ZnO nanowires

Mansoor Ahmad [a,*], M.K. Ahmad [a,**], N. Nafarizal [a], C.F. Soon [a], N.M.A.N. Ismail [a], A.B. Suriani [b], A. Mohamed [b], M.H. Mamat [c]

[a] Microelectronic and Nanotechnology–Shamsuddin Research Centre (MiNT-SRC), Faculty of Electrical and Electronic Engineering, Universiti Tun Hussein Onn Malaysia (UTHM), 86400, Parit Raja, Batu Pahat Johor, Malaysia

[b] Nanotechnology Research Centre, Department of Physic, Faculty of Science and Mathematics, Universiti Pendidikan Sultan Idris, 35900, Tanjung Malim, Perak, Malaysia

[c] NANO-ElecTronic Center (NET) School of Electrical Enginnering, College of Engineering, Universiti Teknologi MARA, 40450 Shah Alam, Salangor, Malaysia

ARTICLE INFO

Keywords:
ZnO nanowires
Piezoelectric potential
VING
Schottky contact
Nanogenerator

ABSTRACT

Here, we report high output voltage generation by employing *p*-type ZnO nanowires as an integral part of vertically integrated nanowire generators (VING). Study has been carried out to generate high piezoelectric voltage by introducing impurities to ZnO nanowires from group V (P, As, Sb) elements which worked as acceptor impurities for intrinsically *n*-type ZnO nanowires by which reverse leakage current through nanowires has been minimized. Three distinct doping concentrations (2, 4 and 6 wt %) of (P, As, and Sb) have been incorporated in ZnO nanowires at room temperature. X-ray photoelectron spectra (XPS) has indicated the presence of Sb_{Zn}–$2V_{Zn}$, $P_{Zn} + 2V_{Zn}$, As_{Zn}–$2V_{Zn}$ complexes acceptors for Sb, P, As doping respectively. Gradual rise in piezoelectric output voltage has been observed. P/ZnO nanowires generated output voltages of 0.9 V, 1.45 V and 1.85 V respectively. For As/ZnO nanowires, output voltages are 1.25 V, 1.51 V and 1.92 V and with Sb doping recorded voltage values are 1.78 V 2.1 V and 2.5 V respectively. To Acquire optimal output voltage doped ZnO nanowires have been further oxidized (with O_2) to mitigate the screening effect and maximum voltage generated by oxidized ZnO are 2.38 V, 2.86 V, and 3.45 V respectively.

1. Introduction

ZnO is one of the most versatile semiconductor material among group II-VI materials. It is direct bandgap material having band gap of 3.36 eV with large exciton binding energy of 60 meV [1–3]. The pertinent reason behind the selection ZnO as a base material to fabricate Nano-scale devices is due to its facile and low cost growth techniques [4]. ZnO is considered to be one of the promising materials, as various morphologies could be prepared efficiently in ambient conditions i.e. nanowires [5], nanosprings [6], nanobelts [7], nanocombs [8] and etc. Single crystal growth at large-scale with any desired shape and orientation could be possible with ZnO. The aforementioned feature made it one of the favorite materials to use in numerous electrical application such as light emitting diodes [9], ultraviolet lasering [10], gas sensors [11–13], and nanogenerators [14]. Piezoelectric nanogenerators has always been the focus of our research [15–17]. Piezoelectric phenomenon is very closely related to the crystal structure. ZnO possess hexagonal crystal structure in which Zn^{+2} and O^{-2} are arranged in a layer by layer fashion one over the other along c-axis. It also exhibits lack of central symmetry, which is supposed to be crucial factor for piezoelectric current generation during an external stress. In normal conditions cations (Zn^{+2}) and anions (O^{-2}) coincide with each other and balance the charge but as the charge balanced condition is being perturbed by tiny external force, charge symmetry disturbs and cations and anions tend to move apart in opposite direction that creates an electric dipole in the crystal. Dipole creation in the ZnO nanowire during an external force

* Corresponding author.
** Corresponding author.
E-mail addresses: Mansoorahmad_28@yahoo.com, mansoor@uthm.edu.my, Mansoor@uthm.edu.my, akhairul@uthm.edu.my (M. Ahmad), akhairul@uthm.edu.my (M.K. Ahmad).

https://doi.org/10.1016/j.vacuum.2022.111130
Received 4 January 2022; Received in revised form 27 April 2022; Accepted 28 April 2022
Available online 1 May 2022

is responsible for piezoelectric potential and the developed potential can last in the crystal only if the external applied force is there so by slight deformation of structure useful piezopotential can be generated which could be used as voltage source.

Z L Wang [6,7] being the pioneer in the field of nanogenerators and his work has always been a motivation to us. Wang [18] has reported various voltage ranges generated by applying different structure configuration for instance generation of 20–50 mV from laterally grown single ZnO on flexible polyimide was the first step then afterwards single ZnO nanowire attached to human finger has produced open circuit voltage of 25 mV during bending and stretching, similarly nanogenerator attached with a body of running hamster has generated voltage peaks up to 100 mV [19]. Special woven nanogenerator [20] has been designed on a wood substrate in which two different kind of fibers have been used, one fiber was covered by ZnO nanowires and other was coated with palladium (Pd) layer, Pd has got high work function than ZnO nanowires and worked as schottky contact. By scavenging frictional energy produced during rubbing of cloths has generated 3 mV pulses. Sheng [21] by using LING (lateral integrated nanowire generator) configuration reported 1.26 V. In LING configuration there is always a limitation that during a continues straining sometime nanowires pluck out from substrate and sometimes the connections with electrodes were lost and output voltage gets disrupted while VING is free from such type of problems. Riaz et al. [22] used *n-type* Si substrates to generate high piezoelectric potential by using high temperature vapor liquid solid technique. Atomic force microscope (AFM) in contact mode has been used to deflect the ZnO nanowire array but the obtained output voltage was around 30–35 mV. High temperature synthesis route was opted which itself a limitation. Similarly, Yue sun et al. [23] designed high performance direct current nanogenerator using carbon as bottom electrode and Au as top electrode and the maximum obtained voltage was 1.6 V but the proposed structure was quite vulnerable and involves high cost. Banerjee et al. [24] proposed complex web like structure that generated maximum piezoelectric voltage of 1.7 V. The basic idea was to eliminate the use of batteries from the system and this web like structure was proposed to work as power source. The approach towards self-powered devices was impressive but only limitation was fabricating procedure which involved number of steps. Recent results are not only impressive in terms of high voltage but also due to its low cost and easy synthesis route. Ongun et al. [25] designed PVDF (poly vinylidene fluoride) nanofibers and Ag doped ZnO nanostructures for energy harvesting applications. The reported voltage range was from 0.5 to 1.5 V, although voltage range was not so high but these nanogenerators could be used in portable electronic systems and self-powered gadgets. Recent study is a continuation of the same goal to achieve high voltage from ZnO nanowires based VING. The recent work has been specially designed to reduce the free charge carriers from ZnO nanowires which is supposed to be a bad factor for piezoelectric nanogenerators [26]. Free charge carriers tend to diminish the piezoelectric potential developed inside the crystal. In first step, minute concentrations of acceptor impurities (P, As and Sb) have been introduced and in second step ZnO nanowires have been oxidized by O_2 to mitigate the screening effects. Screening effect is one of the bottlenecks of piezoelectric nanogenerators [27]. Although *p-type* doping in ZnO nanowires is quite challenging because of its intrinsic donor effects and deep acceptor levels that is why it's not the first choice of the researchers [28], however there are few attempts made by using expansive techniques like radio frequency sputtering [29,30], thermal diffusion [31], pulsed laser deposition [32] and Ion implantation [33]. Recent study is quite unique because facile aqueous route has been opted through which minute concentrations of acceptor impurities have been incorporated in ZnO nanowires at low temperature. It's a hassle free technique and low cost synthesis route. The *Ex situ* doping techniques like, ion implantation and thermal diffusion have considered to be more damaging to ZnO nanowires while *In-situ* doping techniques regarded more safe as far as lattice damage is concerned [34,35]. Although N is considered to be a good choice for *p-type* doping due to its solid solubility and electronic configuration [36] but at there is also an evidence of the poor stability at room temperature i.e. converting back to *n-type* from *P-type* conductivity [37]. Theoretically [38] Sb is suggested to be good *p-type* additive as because it produces (Sb_{Zn}–$2V_{Zn}$) acceptor complex rather than occupying oxygen sites in ZnO to form deep energy levels. Larger in size and mismatched Sb atoms supposed to replace Zn atoms by the creation of two Zn vacancies to form a stable formation at room temperature. Similarly, for P-doping $P_{Zn} + 2V_{Zn}$ complex regarded as more effective configuration than P_O configuration. As because $P_{Zn} + 2V_{Zn}$ supposed to form shallow acceptor levels and provides more hole concentration than P_O configuration in which P_O is supposed to form deep energy levels and provide low hole concentration. P_{Zn} is antisite substitutional P and $2V_{Zn}$ are two zinc vacancies [39]. Study has achieved envisioned results because we have successfully grown As, P and Sb doped ZnO nanowires which generated high piezoelectric voltages.

2Material and methods

We have grown VING structure using ITO (indium tin oxide) coated PET (poly ethylene terephthalate) substrate as bottom electrode, ZnO nanowires as intermediate part and top electrode is gold sputtered electrode. PET substrates were cleaned by deionized water in an ultrasonic bath for 15 min The dried. 0.1 M of Zinc acetate dihydrate [$Zn(CH_3COO)_2{\cdot}2H_2O$] is used to grow seed layer on PET substrate then substrates were annealed at 50 °C for 30 min 1st step of seed layer growth has been repeated 2–3 times. For vertical growth of ZnO nanowires, nutrient solution of hexamethylenetetramine [$C_6H_{12}N_4$] and Zinc nitrate hexahydrate [$Zn(NO3)_2.6H_2O$] has been prepared. PET substrates were immersed upside down in nutrient solution for 3 h at 90 °C. ZnO nanowires morphology and aspect ratio is found to be dependent on temperature and time of growth in nutrient solution and density of the nanowire has been controlled by adjusting the concentration of nutrient solution. The concentration of the solution has been adjusted carefully by using following relation.

$$C = [m / V] \times [1/MV] \quad (1)$$

C is the molar concentration or molarity of the solution, m is the mass of solute in grams V is the volume of the solution in which solute needs to dissolved and MV is the molecular weight in g/mol. Details of growth procedure has been explained in our earlier reports [4,5]. Emscope SC500 is used to sputter Au electrode on top of ZnO nanowires, Ar gas with a pressure 0.1 Torr is being filled in the chamber, 2kv operating voltage is being used to initiate charge irradiation inside the chamber. For P- doped ZnO nanowire zinc phosphate (Zn_3P_2) in powder form is used as dopant. Minute concentration of 2, 4 and 6% wt. has been used. Desired amount of zinc phosphate has been immersed in nutrient solution and solution is stirred for 30 min at 60 °C. For Sb doped ZnO nanowires antimony acetate [$Sb(CH3CO_2)_3$] of analytical grade (98% purity) has been used. Antimony acetate is used as precursor solution for Sb and the concentration of Sb is varied to 2 to 6%wt. precursor was dissolved in deionized water and then mixture is stirred at 60 °C for 30 min and mixture was added to nutrient solution. To incorporate As, pure (99.9%) arsenic in powder form purchased from sigma Aldrich has been used 2,4 and 6%wt. As has been added to directly in nutrient solution and stirred at 60 °C for 30 min. Minute *p-type* impurities (As, P and Sb) have been indicated by XPS and XRD patterns and being well verified by enhanced piezoelectric output voltages. XPS studies have been performed by using PHI 5000 scanning ESCA microprobe using (hv = 1486 eV) and X-ray source was operated at 15 KV, power 25 W, 100 μm spot size. XRD pattern have been obtained by Shimadzu - 6000 X-ray diffractometer having source Cu Kα (λ = 1.54° A). The schematic diagram of VING has been shown in Fig. 1. Minute force of ~100 nN is applied on top electrode to generate piezoelectric inside ZnO nanowires. Picoscope 5204 has been used to measure output voltages generated by

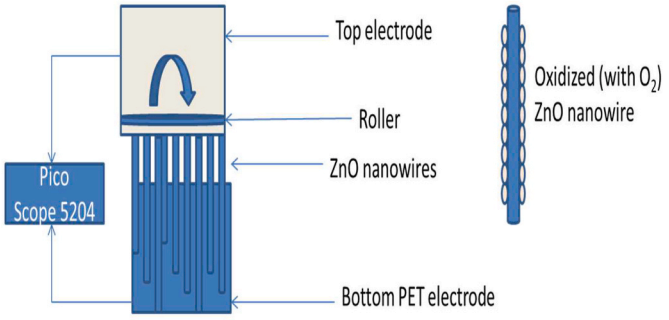

Fig. 1. Schematic diagram of ZnO based VING and oxidized ZnO nanowire.

the structure.

VING structure have been further oxidized with O_2 to mitigate the screening effects during the external stress. To achieve Optimal voltage, VING has been oxidized for 5 h in a sealed chamber at 100 ppm. The oxidation phenomenon has been very well explained in our earlier findings [15] which has significantly minimized the screening effect during external compression.

3Results and discussions

Surface morphologies of pristine ZnO nanowires and doped nanowires have been examined by ESEM images by using Philips XL30. Fig. 2 (a) shows the topographical image of as-grown ZnO nanowires which ensures the vertical growth orientation of nanowires. Fig. 2 (b, c and d) also shown the same trend. Minute dopants have not altered the perpendicular growth orientation but slight variation in diameter range has been observed. SEM images clearly indicated the uniform growth of ZnO nanowires on PET substrate. To examine the diameter distribution of doped and un-doped ZnO nanowires Image J software has been used [40]. Initially, particular SEM image has been selected to measure top surface area of ZnO nanowires. Selected image has been replicated in imageJ software then converted it in 8-bit image. In second step, calibration of scale has been carried out, as imageJ doesn't understand the SEM image scale. In third step, grey image has been obtained by using.

$$A = \pi r^2 \tag{2}$$

Fig. 3 (a) shows histogram representation of diameter distribution of pristine ZnO nanowires, the average diameter range is around 100 nm. The ionic radii for Zn^{+2} is 0.74 A^o and both arsenic and Phosphorus placed on the right in the periodic table exhibiting small atomic radii according to the periodic trends. Arsenic atomic radius is quite close to Zn so diameter of As-doped ZnO nanowires is not much affected [41] but for phosphorus [42] atomic number is 15 so less number of electrons as compared to Zn i.e. electronic repulsion is less and atomic radius is smaller than of Zn so diameter of P-doped nanowires is squeezed a bit (~90 nm) while for antimony due to large number of electrons electronic repulsion is high and atomic radius is larger so diameter range (~110 nm) of Sb-doped ZnO nanowires is bit on larger side [43]. Minute doping concentrations have produced slight change in the diameter rang for all three cases.

Fig. 4 shows the XRD pattern of as-grown and doped ZnO nanowires. Obtained peaks have been matched to standard hexagonal wurtzite structured XRD peaks (JCPDS Card no 36–1451). Doped and un-doped ZnO nanowires have shown preferential growth orientation along c-axis which is quite encouraging. In Fig. 4 (a, b, c) the diffracted pattern of as-grown ZnO nanowires at an angle (2Θ) 31.56°, 34.46°, 47.59°, 56.86° corresponds to crystal planes (100), (002), (102) and (110) respectively. Sharp peaks along (002) plane indicated that most of the nanowires have shown vertical growth orientation. Slight shift in XRD peaks towards the lower angles indicates minute doping of As, P and sb.

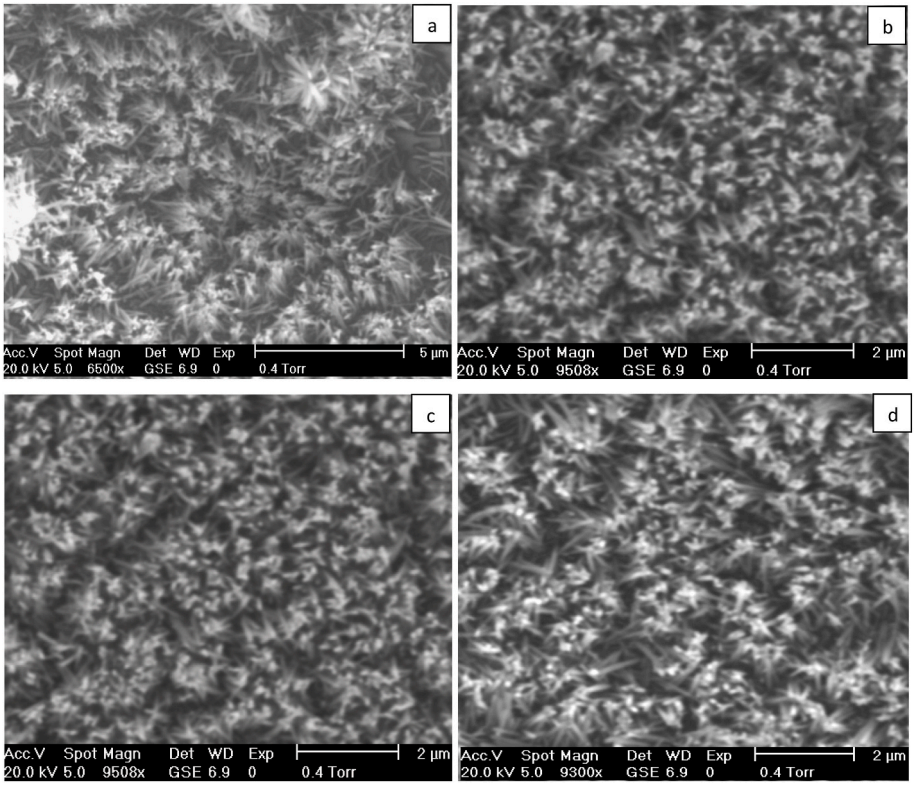

Fig. 2. SEM images of ZnO nanowires, (a) pristine ZnO nanowires, (b) As-doped ZnO nanowires, (c) P-doped ZnO nanowires, (d) Sb-doped ZnO nanowires. binarization technique and in final step by adjusting the contrast of the modified image only top surface area of nanowires has been selected and rest is discarded. Top surface area of nanowires has been calculated by using.

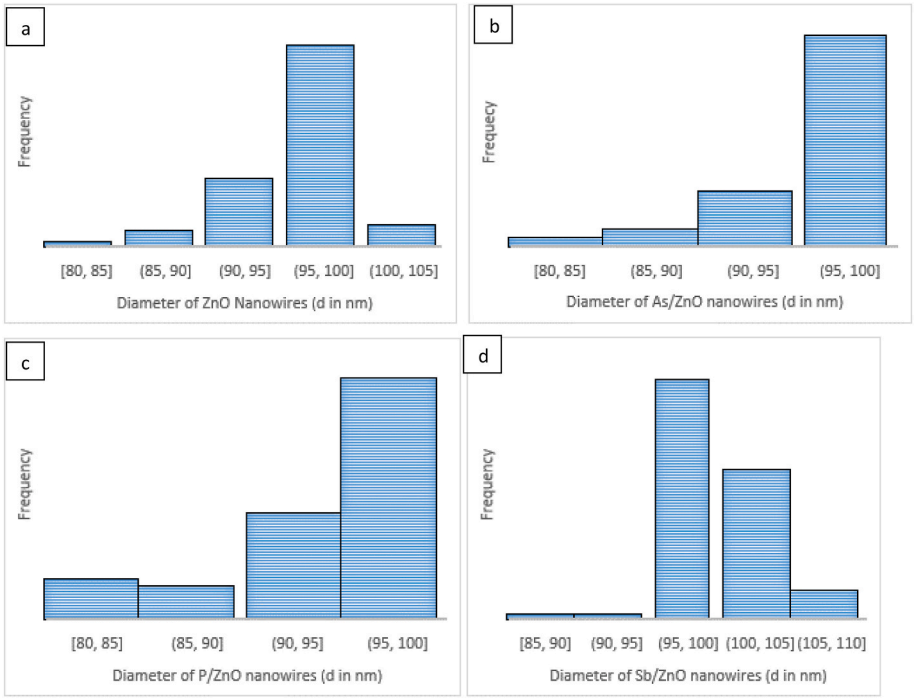

Fig. 3. Histogram showing diameter range of ZnO nanowires, (a) pristine ZnO nanowires, (b) As-doped ZnO nanowires, (c) P-doped ZnO nanowires, (d) Sb-doped ZnO nanowires.

The slight shifting of peaks could be due to internal stress after doping. It could due to interstitial defects, defects due to vacancies or small dislocations. According to Bragg's equation [44] peak positioning is closely related to lattice parameters and shifting in peaks is due to internal stress of the crystal by small ion replacement. It could be small dislocations. XRD results also indicated that there were no secondary peaks corresponding to As, P and Sb were observed. It ensured that the doping concentrations were minute and doped elements have been well incorporated in ZnO nanowires. Dominant peak along (002) plane indicates the vertical growth orientation of ZnO nanowires before and after doping. XRD results are well supported by XPS results. Concentration mapping has been plotted by using Scherrer-Debye equation [45] in which D is the crystallite size (nm), K (0.9) is Scherrer constant ʎ is the wave length (0.15406 nm) of the source used, β is FWHM (full width at half maximum) in radians, Θ is the peak position in radians.

$$D = K \lambda / \beta \cos \Theta \quad (3)$$

Mapping concentration confirms the uniform distribution of P, As, and Sb in ZnO nanowires.

XPS spectra for Zn and O is shown in Fig. 5 (a, b) two peaks at BE 1021.1 eV and 1043.5 eV are related to Zn $2p_{3/2}$ and Zn $2p_{1/2}$ states, respectively. Fig. b shows the O spectra in which peaks at BE at 529.5 eV and at 532 eV are due the presence oxygen in ZnO. Spectra corresponds to as-grown ZnO nanowires. High resolution XPS-spectra has been analyzed to elucidate the presence of arsenic in ZnO nanowires. As3d XPS spectra has been deconvoluted into two peaks, peak at binding energy 41.3eV has been deconvoluted doublets as shown in Fig. 5(d), similarly peak at binding energy at 43.5 eV has been deconvoluted representing $As3d_{5/2}$ – $As3d_{3/2}$. The peak at binding energy at 47.5 eV could be attributed to As–O bonding [46,47]. The peaks at BE 42 V has been due to amphoteric contribution of arsenic and represents Zn–As bonding [48]. Similarly, it has been reported earlier [49] that peaks at BE 43–45 eV are related to As_{Zn}–$2V_{Zn}$ shallow acceptor complexes. Substitutional defect produced by arsenic and generating two zinc vacancies are supposed to from shallow stable acceptor levels that supports *p-type* doping in ZnO nanowires. These supposed to generate more holes rather than O_{As} defect which usually form deep acceptor level and provide low hole concentration [50]. XPS is also very effective technique to investigate chemical state of the dopant. As in the P doping, the small peak at BE 133.5 eV attributes incorporation of P in ZnO nanowires. It has been reported earlier [51] that peak at 129 eV corresponds to Zn–P bonding surrounded by Zn atoms. The peak at BE 139.2 eV attributes Zn3s state. Experimentally obtained values are in agreement with theoretically predicted values [52]. It has been explained theoretically that P-doping in ZnO nanowires creates shallow acceptor level. Substitutional defect generated by P atoms and generating two Zn vacancies is regarded as an effective configuration for *p-type* doping. $P_{Zn} + 2V_{Zn}$ complex is formed by antisite substitutional P(Zn) and zinc vacancies (V_{Zn}). The configuration has raised the internal resistance of the ZnO nanowires and generated sufficient holes inside ZnO nanowires which captured free electrons. Argument has been well supported by the output voltage peaks shown in Fig. 6 showing gradual rise in output voltage which is due to enhancement of internal resistance of nanowires and shortage of reverse leakage current through them [14].

XPS spectra collected for Sb doped ZnO nanowires has been shown in Fig. 4(e) and atoms and peak appearing at BE 539.0 eV attributes the presence of Sb $3d_{3/2}$. Large peak at BE 529.5 V has been deconvoluted in two small peaks as shown in Fig. 5 (e) the large peak is due to the overlapping of O 1s and Sb $3d_{5/2}$. Interestingly, peak at BE 539.0 eV corresponds Sb $3d_{3/2}$ also could be observed again in the spectra. Obtained peaks matched to theoretically predicted values [53]. Theoretically, Sb supposed to replace Zn by introducing two zinc vacancies. It leads to complex shallow acceptor level Sb_{Zn}–$2V_{Zn}$. It has been well manifested by output voltage graphs (Figs.6–8) maximum voltage peaks have been appeared in Sb doped voltage spectra. Pertinent reason behind the large piezoelectric output voltage is the capturing of free moving electrons inside ZnO nanowires by these shallow acceptor levels.

Fig. 6 (a) confirms the generation of piezoelectric potential and its deliverance at output stages. In Fig. 6(b) histogram showing voltage occurrence of the output voltage, most of the positive voltage values are around 0.6 V and negative voltage are around −0.6 V. It also ensures the schottky contact between ZnO nanowires and upper gold sputtered electrode. Schottky contact is quite crucial factor in piezoelectric

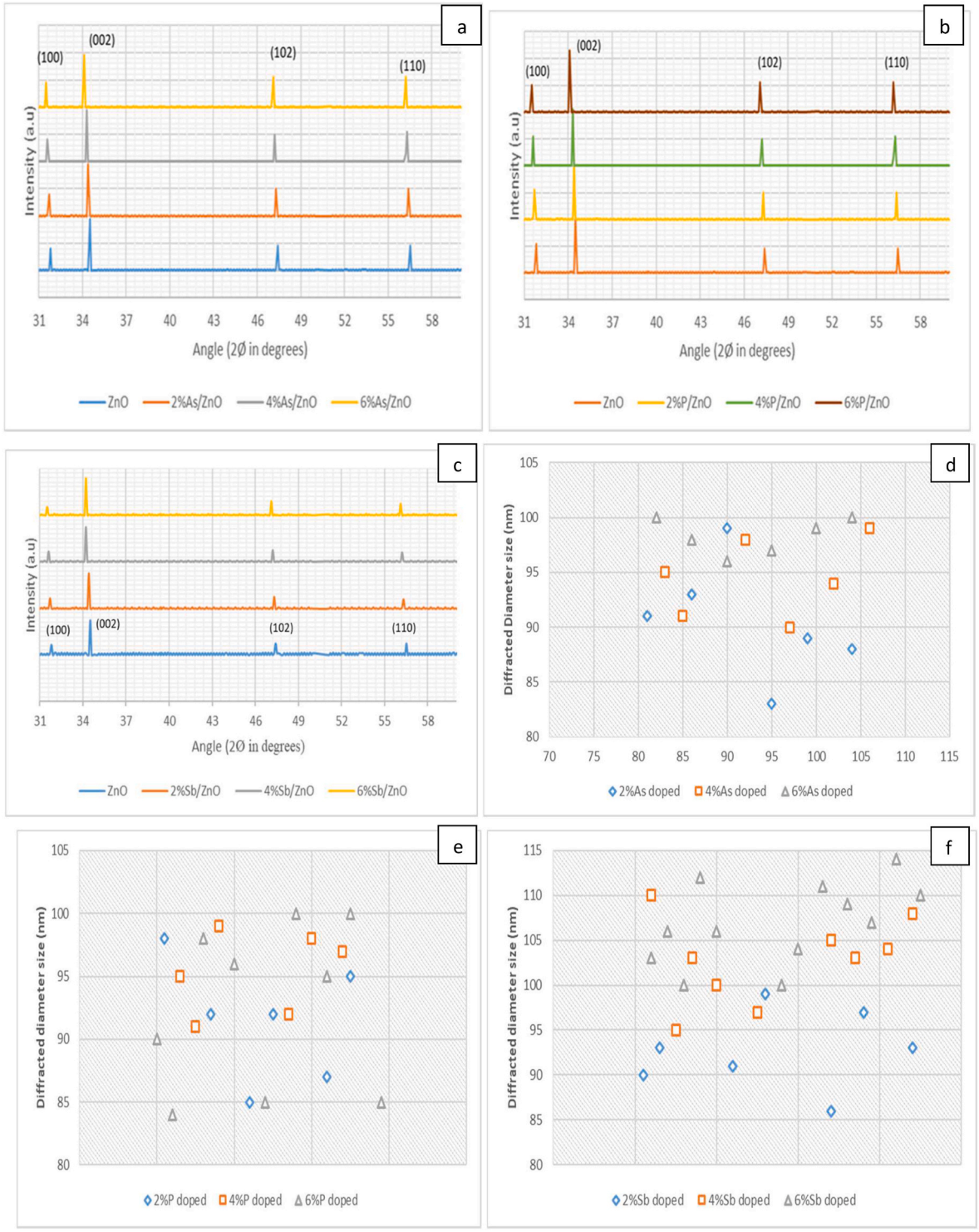

Fig. 4. XRD pattern of vertically grown ZnO nanowires, (a) As-doped ZnO nanowires, (b) P-doped ZnO nanowires (c) Sb-doped ZnO nanowires, (d–f) doping concentration map of As, P and Sb in ZnO nanowires.

nanogenerators [4,5], as it only allows the current to flow in one direction i.e. through external circuit and tend to stop the flow of current through nanowires. Fig. 6 (c, d and e) shows the output voltage spectra for P-doped ZnO nanowires, as its already been discussed earlier that group V elements are supposed to be good candidates for *p-type* doping. Another reason for selecting P, As and Sb are their electron affinities. For instance, Phosphorus has an electron affinity of 0.707 eV and it has been clearly manifested in voltage graphs voltage has been gradually enhance as the doping concentration is increased from 2% to 6%wt. pertinent reason of voltage rise is the creation of shallow level defect $P_{Zn} + 2V_{Zn}$ as indicated by XPS which generated holes in the structure and free moving electrons are being trapped in the holes. Free moving electrons inside nanowires depletes the piezoelectric potential and consequently output voltage is decreased. Electron affinity has also played a crucial role in attracting the free moving electrons inside ZnO nanowires and reduced the conducting channels inside them. Generally, the conduction of nanowires is associated with discrete energy levels also called quantized conducting channels and the conductance of the nanowires referred as

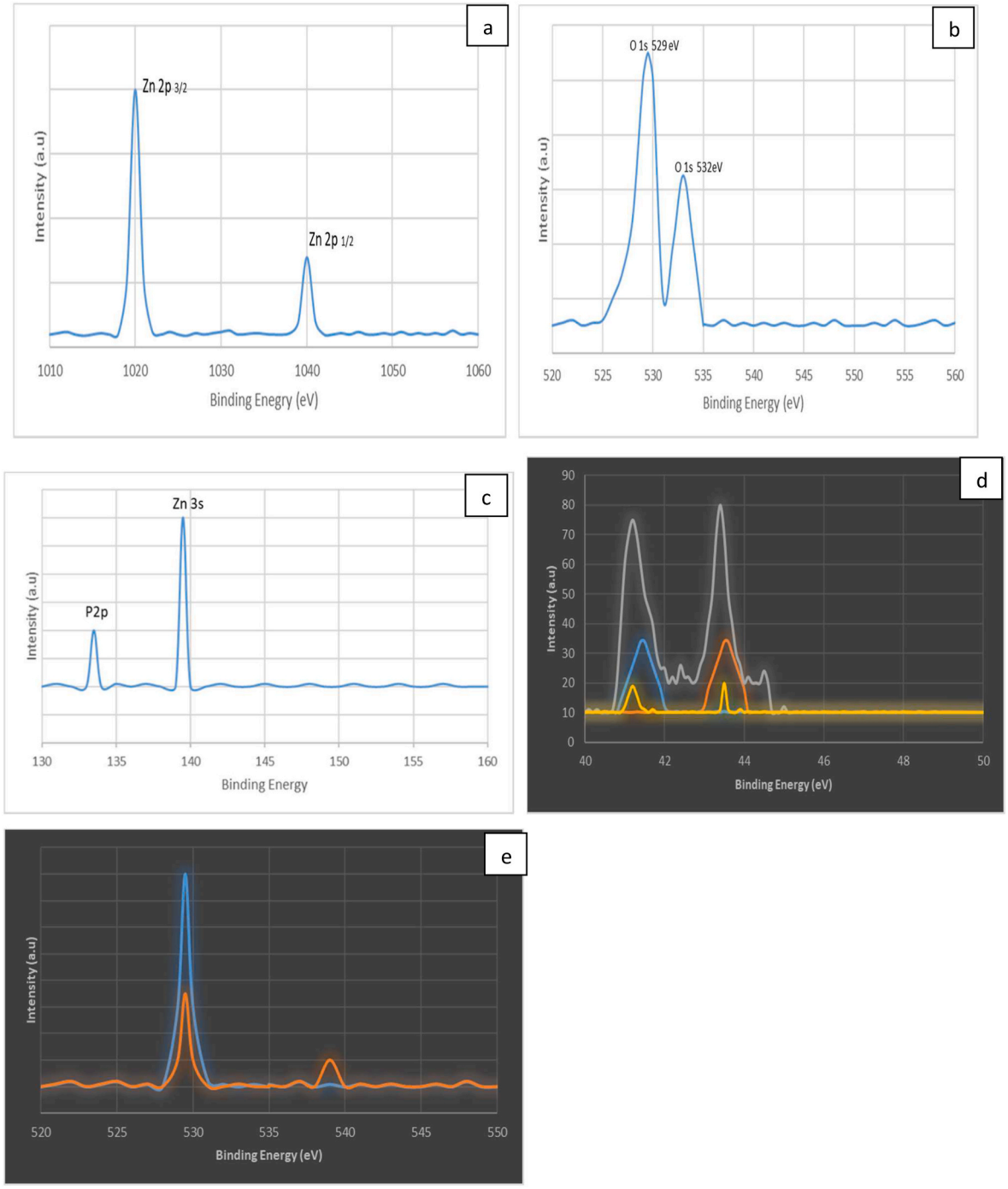

Fig. 5. XPS spectra, (a) Zn 2p (b) O 1s, (c) P-doped ZnO nanowires, (d) As-doped ZnO nanowires, (e) Sb-doped ZnO nanowires.

quantum conductance G which is integral multiples of the factor $e^2/2$ h [54].

Schottky contact plays a vital role in deliverance of developed piezopotential at the output stages [55]. During an external stress, charges tend to accumulate on either side of the nanowires and create electric field inside the crystal structure. Piezoelectric potential is basically the consequence of these electric dipoles. In piezotronic devices, the goal is to deliver the developed piezoelectric potential at output stages through metal electrode. Ø is the potential barrier height which is difference of the work function of the metal and electron affinity of semiconductor. The purpose of this potential barrier is to allow the electrons to move in one direction only i.e. through the external circuit and stops their flow through the nanowires. When external force is applied, barrier height gets reduced due to charge accumulation of on either ends of the semiconductor as shown in schematic Fig. 7. Developed piezoelectric potential works as charge pump for the electrons and electrons tend to flow through the external circuit. Schottky barrier at the interface ensures the flow of current through nanowires and stops reverse leakage current through nanowires.

In VING, when a force is applied on top of nanowires fermi level and conduction band of the top electrode rises as compared to bottom electrode. Due to this potential gradient developed between top and bottom electrode, electrons move from top to bottom electrode through external load. This will eventually rise the fermi level and conduction band of the bottom electrode. The flow of electrons continue until there is an equilibrium establishes between top and bottom electrode. When

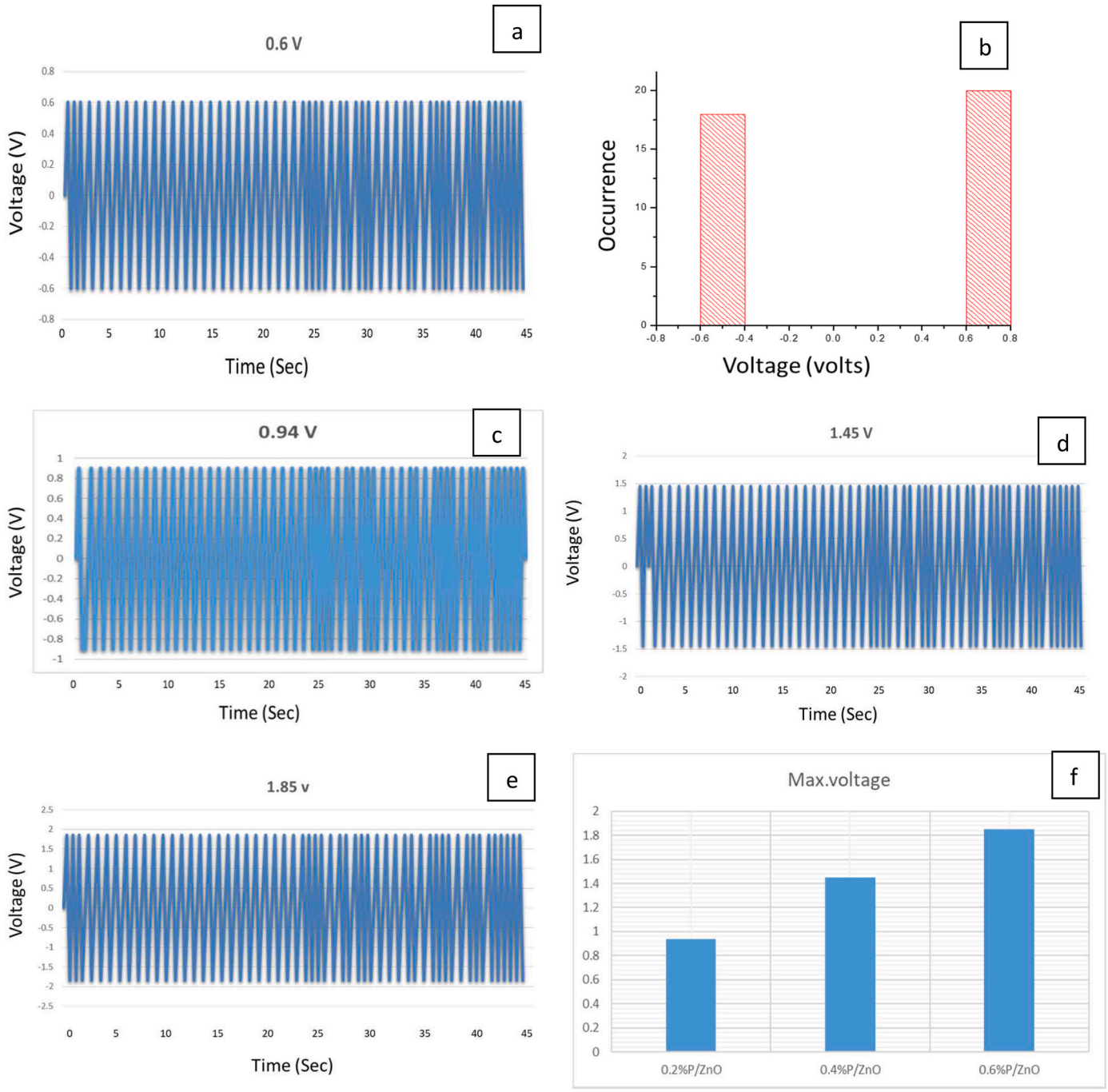

Fig. 6. output voltage values generated by ZnO nanowires based VING, (a) as-grown, (c) 2%P/ZnO (d) 4% P/ZnO (e) 6% P/ZnO (b) voltage histogram, (f) column bar graph showing sequential rise in the voltage with respect to doping concentrations.

an external force is removed piezoelectric potential inside nanowire collapse and accumulated electrons at the bottom electrode flow back through external circuit towards the top electrode. Electron affinity of the semiconductor must be less than the work function of metal used. Au (gold) has work function of 5.1 eV and ZnO has an electron affinity of 4.5 V. As the difference between electron affinity and work function of metal gets larger the chances for electrons to surpass the barrier diminishes. Schottky contact acted as barrier and it allowed the electrons to flow in one direction only i.e. through external circuit not through the nanowires [56]. For *n-type* semiconductor, ideally the donor level should be just below the conduction band so that enough electrons would be available for conduction but if the donor level is pushed far from conduction band edge and near to valance band edge it acts as deep donor level which is not conducive for n-type conductivity as shown in Fig. 8(a and b). For an ideal *p-type* doping, the acceptor levels are supposed to be near the valance band maxima so that it can trap the free electrons efficiently while if the acceptor level is formed far from conduction band maxima it cannot the capture the electrons easily and it is regarded as deep acceptor level. That is why shallow acceptor levels are regarded more significant as compared deep acceptor levels as shown in Fig. 8 (c, d). Eg is energy band gap between conduction band minima and valance band maxima Ec is denoted for conduction band minima and Ev for valance band maxima [57].

Fig. 9 (a) represents periodic piezoelectric voltage generation by pristine ZnO nanowires and Fig. 7 (b) confirms the voltage occurrence range. The electron affinity for arsenic is 0.807 eV and output voltage

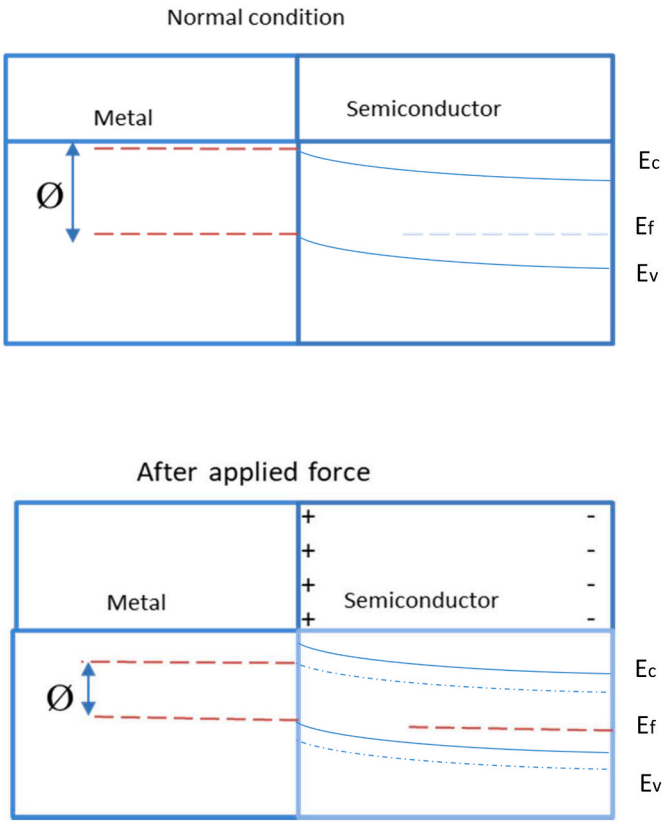

Fig. 7. Schematic energy band-diagram of metal-semiconductor interface.

produced by As-doped ZnO nanowires verified it. Slight rise in output voltage as compared to P-doped ZnO nanowires is due to the small difference of electron affinities. Max. voltage produced by 6% P/ZnO nanowires is 1.85 V and same concentration of arsenic has produced output voltage of 1.92 V. Creation of shallow acceptor levels as indicated by XPS results have been well accredited by voltage enhancement graphs.

Fig. 10 (a) represents the piezoelectric voltage generated by undoped ZnO nanowires and Fig. 10 (b) verified the voltage occurenece range 0.64 V for positive voltage and −0.64 V for negative voltage. Electron affinity for Sb is 1.07 eV which is greater than P and As so output voltage follows it and maximum voltage generated by 6% Sb/ZnO is 2.5 V. As discussed earlier, the quantum conductance G of nanowires is closely related to the availability of free electronics inside ZnO nanowires. Sb_{Zn}–$2V_{Zn}$ complex have generate holes that captured free moving electrons and have reduced reverse leakage current through the nanowires. Consequently, output voltage has been enhanced gradually as shown in Fig. 10(c–e).

Gao. Y [58] theoretically explained the screening effect phenomenon. It has been the bottleneck in piezoelectric nanogenerators. Theoretically, it has been predicted that piezoelectric voltage can be enhanced significantly, if the screening effect during external stress is reduced. Concept has been established by using finite element analysis involving various differential equations. Screening effect phenomenon is due to the free moving electrons available in the conduction band and during an external stress, due to the bending of the nanowires they are attracted towards the positive side electric dipoles and tend to deplete the piezoelectric potential. Yang [59] has experimentally verified the screening effect phenomenon and has observed that in a dense growth of vertically aligned ZnO nanowires there is also a tunneling phenomenon occurring and depleting the piezoelectric potential. During the bending electrons are jumping from one wire to the neighboring wires and depleting the piezoelectric potential. Yang et al. has shown that nanowire in the middle of vertically aligned structure has generated less potential as compared to the nanowire at the edges or the corners i.e. due to the tunneling effect. It has been established in our earlier reports [13–16] that by surface modification of ZnO nanowires the screening effect could be reduced. ZnO nanowires have with oxidized with O_2 gas for 5 h in a sealed chamber at100 ppm. The difference in between the piezoelectric voltage generated by oxidized and un-oxidized ZnO nanowires is clear from Fig. 11 (e). Oxygen molecules adsorbing on

$$O_2 + e^- \rightarrow O_2^- \quad (3)$$

ZnO nanowire surface by capturing free electrons creates layer on the outer surface of nanowires [48]. The outer layer foils the electron tunneling during a continuous external straining. By capturing free electrons concentration of free charge carriers would be reduced. Reduction of free charge carriers has reduced the reverse leakage current through the nanowires and last but not least O_2 molecules have given rise to edge effect as well. Edge effects has enhanced the internal resistance of the nanowires i.e. due to scattering phenomenon. Enhancement of internal resistance due to internal scattering will tend to minimize the flow of any residual charge carriers. Enhanced piezoelectric.

Voltage as shown in Fig. 11(a–c) has verified that reverse leakage current has been further reduced by surface modification of ZnO nanowires. To ensure the optimal output voltage, variable load resistance (2–12 MΩ) has been employed as shown in Fig. 11 (d). Maximum voltage 3.45 V has been recorded.

In comparison with earlier findings as discussed in the introduction recent study stands out unique. Cost effective route has been adopted to obtain high output voltage under ambient conditions. In Future, electric vehicles will play a pivotal role in producing carbon free environment globally. ZnO nanowires base nanogenerators could be vital integral part of future EV. These tiny mechanical transducers not only could be used to convert small mechanical energies of EV in useful electrical pulses but also could be used to replace the conventional batteries. High voltage values could be by achieved by combining nanogenerators in

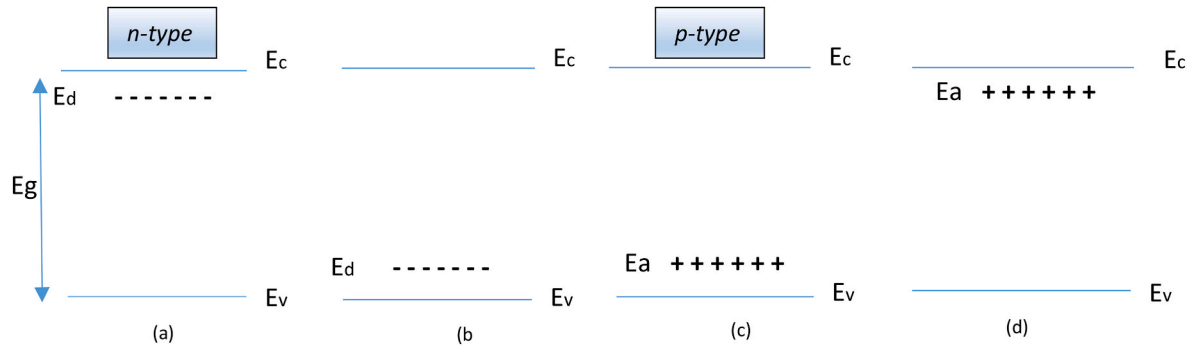

Fig. 8. Schematic band diagram indicating shallow acceptor and donor levels.

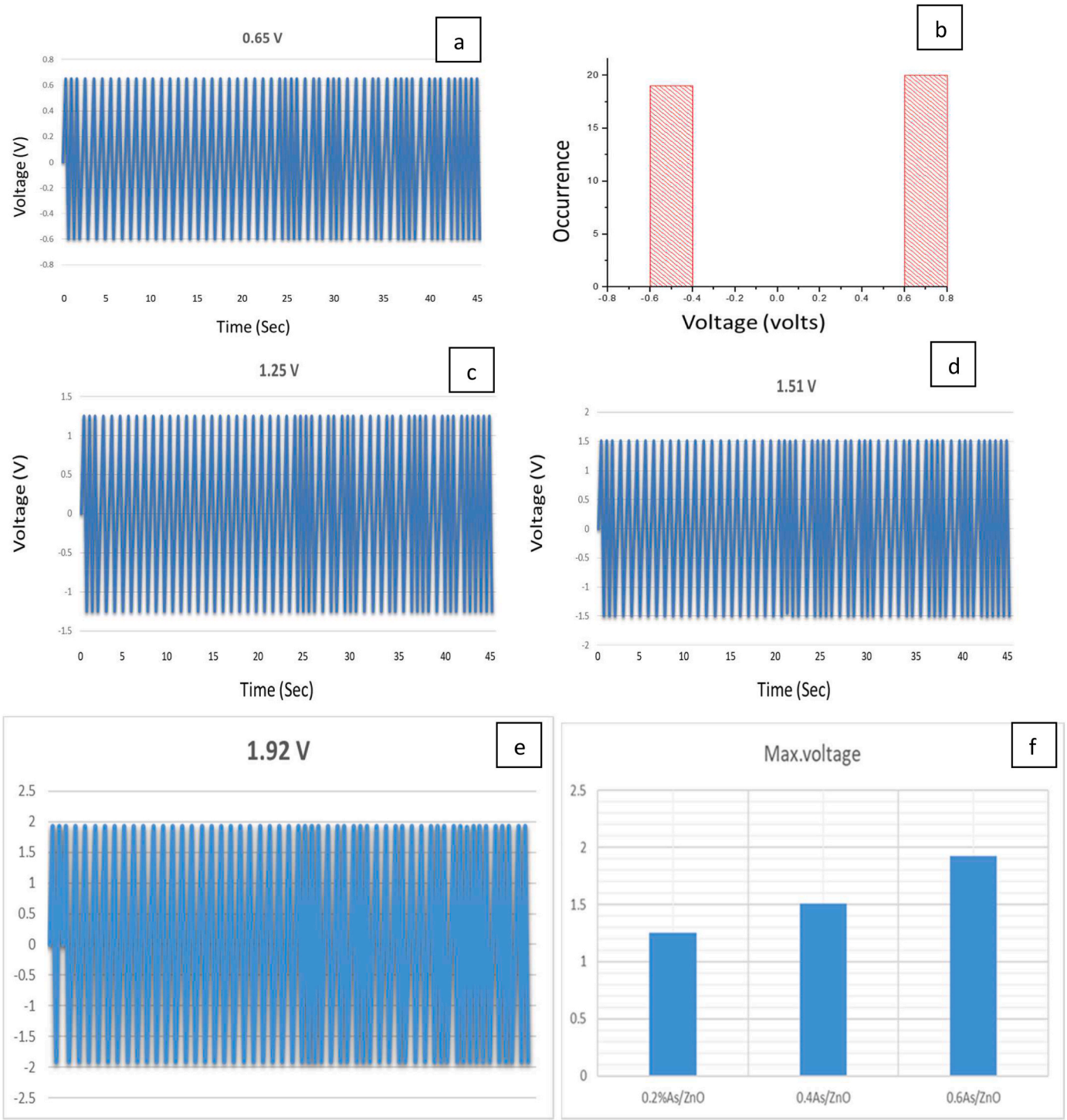

Fig. 9. output voltage values generated by ZnO nanowires based VING, (a) as-grown, (c) 2%As/ZnO (d) 4% As/ZnO (e) 6% As/ZnO (b) voltage histogram, (f) column bar graph showing sequential rise in the voltage with respect to doping concentrations.

series. In the recent case, by combining 3 to 4 nanogenerators in series more than 12 V could be achieved. Recent results are quite competitive and fine addition to tally of the nanogenerators.

4- Conclusions

We have successfully grown *p-type* doped ZnO nanowires at room temperature. Minute doping concentrations of P, As and Sb have successfully incorporated in ZnO nanowires to generate high piezoelectric potential. XPS results indicated the presence of desired $P_{Zn} + 2V_{Zn}$, $As_{Zn}–2V_{Zn}$ and $Sb_{Zn}–2V_{Zn}$ acceptor levels. and XRD results have indicated the minute presence of doped impurities and it was well verified by the output voltage graphs. The generation of piezoelectric voltage has been enhanced first by minute impurity doping and second by reducing the screening effects. ZnO nanowires have been oxidized with O_2 molecules, it created layer on outer surface of ZnO nanowires. The deposited layer minimized the screening effect during external stress. Maximum voltages generated by P/ZnO nanowires, As/doped and Sb/ZnO nanowires are 1.85 V, 1.92 V and 2.5 V respectively and with oxidized structures voltages have been further enhanced to 2.38 V, 2.86 V, and

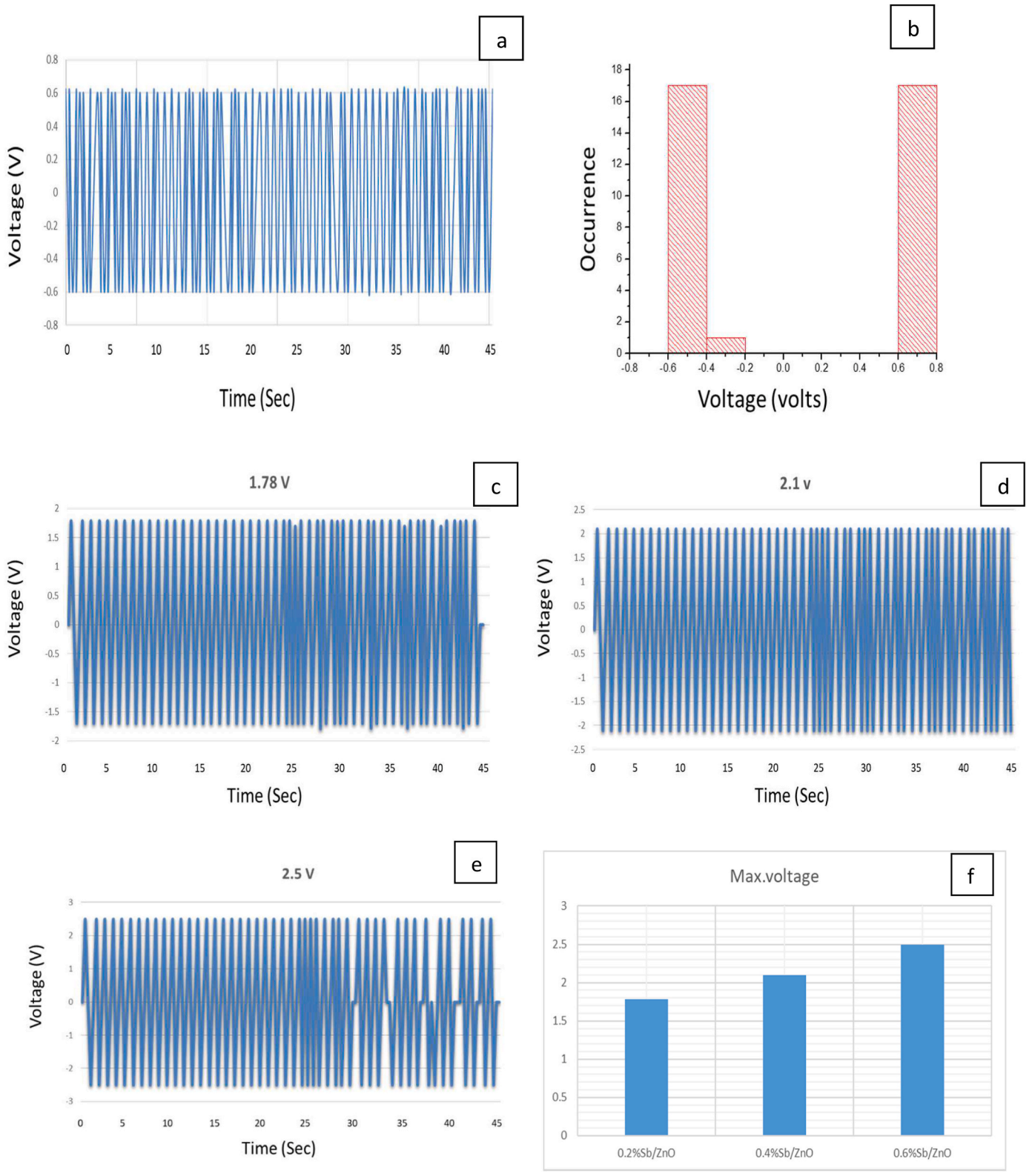

Fig. 10. output voltage values generated by ZnO nanowires based VING, (a) as-grown, (c) 2%Sb/ZnO (d) 4% Sb/ZnO (e) 6% Sb/ZnO, (b) voltage histogram, (f) column bar graph showing sequential rise in the voltage with respect to doping concentrations.

3.45 V respectively. These tiny mechanical transducers are proposed to be used as integral part of self-powered devices. Proposed VING is highly recommended for a sustainable and longtime high output voltage.

CRediT authorship contribution statement

Mansoor Ahmad: Investigation, Methodology, Writing – original draft, Writing – review & editing. **M.K. Ahmad:** Resources, Data curation, Funding acquisition. **N. Nafarizal:** Project administration. **C.F.**

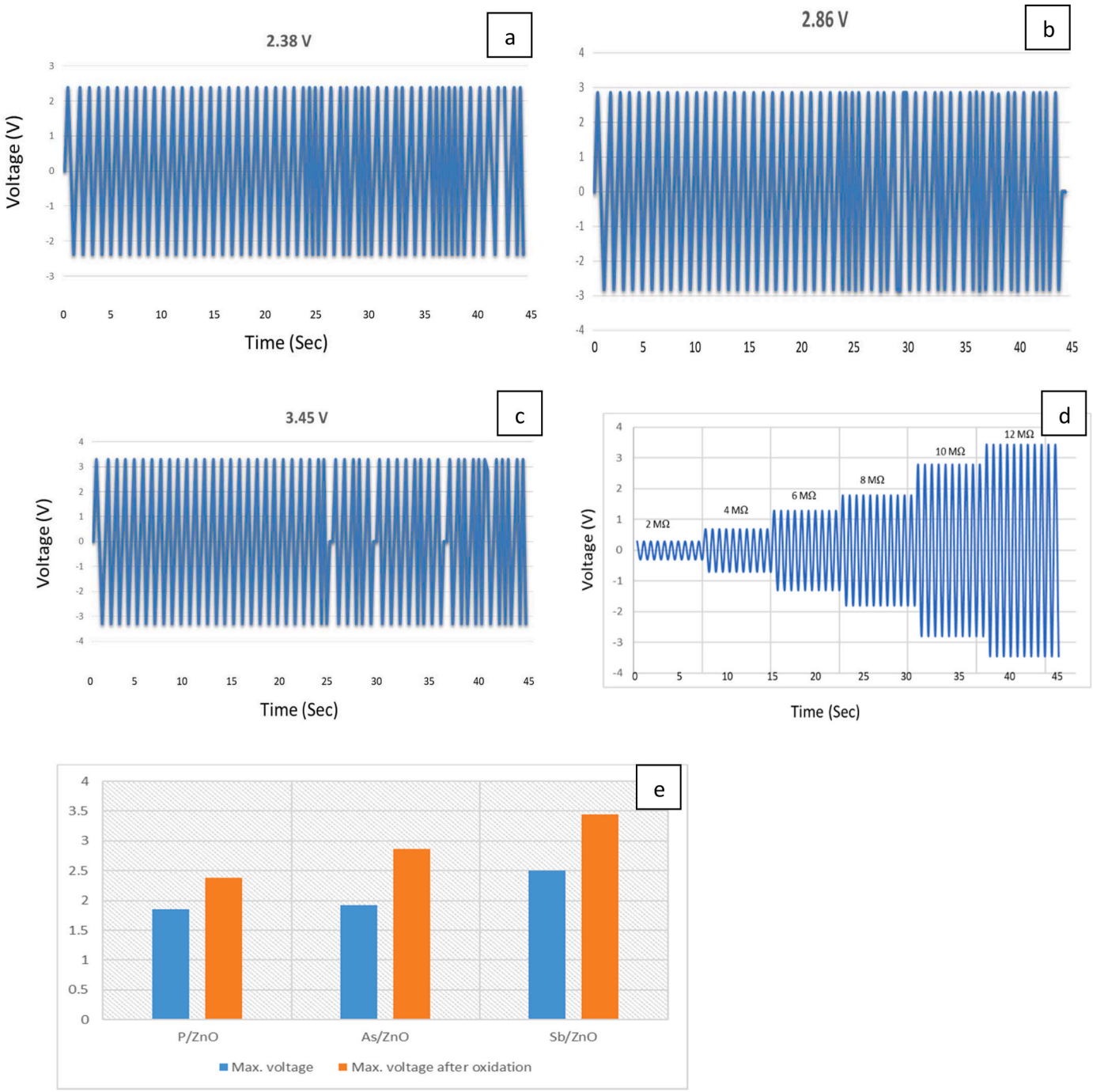

Fig. 11. output voltage values generated by ZnO nanowires based VING oxidized for 5 h, (a) 6%As/ZnO, (b) 6%P/ZnO (c) 6% Sb/ZnO (d)Voltage increment by changing load resistance, (e) voltage comparison for all three cases with and without oxidation.

Soon: Formal analysis. **N.M.A.N. Ismail:** Methodology. **A.B. Suriani:** Data curation. **A. Mohamed:** Funding acquisition. **M.H. Mamat:** Data curation.

Declaration of competing interest

The authors declare that they have no known competing financial interests or personal relationships that could have appeared to influence the work reported in this paper.

Acknowledgement

The authors acknowledge the financial support provided by the Postdoctoral Research Grant and research fund grant tier 1 vot no. H838 from Universiti Tun Hussein Onn (UTHM) Malaysia. The authors are grateful to Dept. of Applied science, UWE, Bristol, UK for extending their experimental facilities.

References

[1] Z.L. Wang, Mater. Sci. Eng. R 64 (2009) 3.
[2] S.J. Pearton, W.T. Lim, J.S. Wright, L.C. Tien, H.S. Kim, D.P. Norton, H.T. Wang, B. S. Kang, F. Ren, J. Jun, J. Lin, A. Osinsky, J. Electron. Mater. 37 (2008) 1426.

[3] M.H. Huang, Y. Wu, H. Feick, N. Tran, E. Weber, P. Yang, Adv. Mater. 13 (2001) 113.
[4] M. Ahmad, J. Kiely, R. Luxton, Sensing and Bio Sensing Research, 2016, p. 7.
[5] M. Ahmad, J. Kiely, R. Luxton, Indian J. Eng. Mater. Sci. (2014) 21.
[6] X.Y. Kong, Z.L. Wang, Nano Lett. 3 (2003) 1625.
[7] X.Y. Kong, Z.L. Wang, Appl. Phys. Lett. 84 (2004) 975.
[8] P.X. Gao, Y. Ding, W.J. Mai, W.L. Hughes, C.S. Lao, Z.L. Wang, Science 309 (2005) 1700.
[9] M.H. Huang, S. Mao, H. Feick, H.Q. Yan, Y.Y. Wu, H. Kind, E. Weber, R. Russo, P. D. Yang, Science 292 (2001) 1897.
[10] X.W. Sun, J.Z. Huang, J.X. Wang, Z.A. Xu, Nano Lett. 8 (2008) 1219.
[11] M. Jabeen, M. Iqbal, M. Ahmad, Sens. Bio. Sens. Res. 25 (2019) 100293.
[12] Yuanjie Su, G. Xie, T. Huiling, et al., Nano Energy 47 (2018) 316–324.
[13] Yuanjie Su, T. Yang, X. Zhao, et al., Nano Energy 74 (2020) 104941.
[14] M. Ahmad, J. Kiely, R. Luxton, J. Phys. Chem. Solid. (2017) 104.
[15] M. Ahmad, M. KAhmad, N. Nafarizal, Mater. Res. Express 7 (2020), 095004.
[16] M. Ahmad, M.K. Ahmad, N. Nafarizal, C.F. Soon, A.B. Suriani, Vacuum 182 (2020) 109565.
[17] M. Ahmad, M.K. Ahmad, N. Nafarizal, Bull. Mater. Sci. 43 (2020) 267.
[18] V. Nguyen, R. Zhu, R. Yang, Nano Enegy 14 (2015) 49.
[19] R.S. Yang, Y. Qin, C. Li, G. Zhu, Z.L. Wang, Nano Lett. 9 (2009) 1201.
[20] B. Suo, L. Zhanga, Q. Xua, Z. LWang, Nano Energy 2 (2013) 749.
[21] M. Riaz, J. Song, O. Nur, Z.L. Wang, Adv. Funct. Mater. 6 (2010) 1.
[22] Y. Sun, Y. Zheng, R. Wang, J. Fan, Y. Liu, Chem. Eng. J. 426 (2021) 131262.
[23] S. Banerjee, S. Bairagi, S.W. Ali, Energy 244 (2022) 123102.
[24] M.Z. Ongun, S. Oguzlar, U. Kartal, M. Yurddaskal, O. Cihanbegendi, Solid State Sci. 122 (2021) 106772.
[25] S. Shi, Z. Pan, Yu Cheng, Y. Zhai, Y. Zhang, X. Ding, Compos. Sci. Technol. 219 (2022) 109260.
[26] M. Ahmad, M.K. Ahmad, N. Nafarizal, Microelectron. Eng. 248 (2021) 111614.
[27] X. Liu, J. Zhang, X. Guo, S. Wang, Nanoscale 2 (2010) 1178.
[28] A.P. Bhirud, S.D. Sathaye, R.P. Waichal, L.K. Nikam, B.B. Kale, Green Chem. 14 (2012) 2790–2798.
[29] D.C. Look, G.M. Renlund, R.H. Burgener, J.R. Sizelove, Appl. Phys. Lett. 85 (2004) 5269.
[30] A. Kumar, M. Kumar, B.P. Singh, Appl. Surf. Sci. 256 (2010) 7200.
[31] E. Przeździecka, E. Kamińska, K.P. Korona, E. Dynowska, W. Dobrowolski, R. Jakieła, Ł. Kłopotowski, J. Kossut, Semicond. Sci. Technol. 22 (2007) 10.
[32] V. Vaithianathan, B.-T. Lee, S.S. Kim, Appl. Phys. Lett. 86 (2005), 062101.
[33] G. Braunstein, A. Muraviev, H. Saxena, N. Dhere, V. Richter, R. Kalish, Appl. Phys. Lett. 87 (2005) 192103.
[34] F. Fang, D. Zhao, X. Fang, J. Li, Z. Wei, S. Wang, J. Wu, X. Wang, J. Mater. Chem. 21 (2011) 14979.
[35] H. He, S. Lin, G. Yuan, L. Zhang, W.F. Zhang, L. Luo, Y.L. Cao, Z. Ye, S.T. Lee, J. Phys. Chem. C 115 (2011) 19018.
[36] J.C. Fan, K.M. Sreekanth, Z. Xie, S.L. Chang, K.V. Rao, Prog. Mater. Sci. 58 (2013) 874–985.
[37] Z.Z. Ye, H.P. He, L. Jiang, Nano Energy 52 (2018) 527–540.
[38] W.J. Chen, J.K. Wu, J.C. Lin, S.T. Lo, H.D. Lin, D.R. Hang, M.F. Shih, C.T. Liang, Y. H. Chang, Nanoscale Res. Lett. 1 (2013) 313.
[39] M.P. Lu, J.H. Song, M.Y. Lu, M.T. Chen, Y.F. Gao, L.J. Chen, Z.L. Wang, Nano Lett. 9 (2009) 1223.
[40] C.A. Schneider, W.S. Rasband, K.W. Eliceiri, NIH image to Image, J Nat. Methods 9 (2012) 671.
[41] D. Snigurenko, R. Jakiela, E. Guziewicz, E. Przezdziecka, M. Stachowicz, J. Alloys Compd. 582 (2014) 594.
[42] Jingyun Gao, Qing Zhao, Yanghui Sun, Li Guo, Jingmin Zhang, Dapeng Yu, Nanoscale Res. Lett. 6 (2011) 45.
[43] Sung-Doo Baek, Pranab Biswas, Yun Jong-Woo Kim, ACS Appl. Mater. Inter. 8 (2016) 13018.
[44] R. Kumari, A. Sahai, N. Goswami, Nat. Sci.: Mater. Int. 25 (2015) 300–309.
[45] Y. Zhang, A. Apostoluk, C. Theron, T. Cornier, Sci. Rep. 9 (2019) 11959.
[46] M. Ding, B.H.W.S. De Jong, S.J. Roosendaal, A. Vredenberg, Geochem. Cosmochim. Acta 64 (2000) 1209.
[47] H. Guan, X. Xia, Y. Zhang, F. Gao, W. Li, G. Wu, X. Li, G. Du, J. Phys. Condens. Matter 20 (2008) 292202.
[48] J.C. Fan, C.Y. Zhu, S. Fung, Y.C. Zhong, K.S. Wong, Z. Xie, G. Brauer, W. Anwand, W. Skorupa, C.K. To, B. Yang, C.D. Beling, C.C. Ling, J. Appl. Phys 106 (2009), 073709.
[49] H.A. Budz, M.C. Biesinger, R.R. LaPierre, J. Vac. Sci. Technol. B: Microelectron. Nanometer Struct. 27 (2009) 637.
[50] G. Du, Y. Cui, X. Xiaochuan, X. Li, H. Zhu, B. Zhang, Y. Zhang, Y. Ma, Appl. Phys. Lett. 90 (2007), 073709, 243504.106, 2009.
[51] S. Limpijumnong, S. Zhang, S.-H. Wei, C. Park, Phys. Rev. Lett. 92 (2004) 155504.
[52] V. Vaithianathan, K. Asokan, J.Y. Park, S.S. Kim, Appl. Phys. A 94 (2009) 995.
[53] W.J. Lee, J. Kang, K.J. Chang, Phys. Rev. B 73 (2006), 024117.
[54] S.K. Pandey, S.K. Pandey, V. Awasthi, M. Gupta, U.P. Deshpande, S. Mukherijee, Appl. Phys. Lett. 103 (2013), 072109.
[55] Z.L. Wang, R. Yang, Jun Zhou, Y. Qin, Chen Xu, Sheng Xu, Materials Science and Engineering R 70, 2010, pp. 320–329.
[56] X. Sheng, Q. Yong, Chen Xu, Yaguang, Z.L. Wang, Nat. Nanotechnol. 46 (2010) 366.
[57] B.G. Shohany, A. Khorsand, Ceram. Int. 46 (2020) 5507.
[58] A.T. Tilke, F.C. Simmel, H. Lorenz, R.H. Blick, Phys. Rev. B 68 (7) (2003), 075311.
[59] Y. Gao, Z.L. Wang, Nano Lett. 9 (2009) 1103–1110.